

THE APPLICATION OF HIGH-RESOLUTION SEM-EDX COMPOSITIONAL MAPPING TO THE TECHNOLOGICAL STUDY OF ANCIENT CERAMICS: A CASE STUDY ON ITALIAN MAIOLICA

Nigel Meeks¹ and Michael Tite²

¹ Department of Scientific Research, The British Museum
E-mail: nmeeks@britishmuseum.org

² Emeritus Professor, University of Oxford, School of Archaeology
E-mail: michael.tite@rlaha.ox.ac.uk

INTRODUCTION

The routine application of scanning electron microscopy with energy dispersive X-ray spectrometry (SEM-EDX) for high resolution mapping, analysis and imaging to the study of ancient ceramics is exemplified here by the study of 15th-17thC Italian Maiolica (see type in Figure 1 upper).



Figure 1. Upper: an example of maiolica Tondino dish with 'Berrettino' decoration, Faenza c. 1535/40 (image from web auction catalogue. Koller Auctions, 19 September 2016); lower: detail of the surface of a sherd (no 5) of similar pattern.

This ceramic material offers a complex mineralogical microstructure and chemistry within the coloured glaze on the fired ceramic bodies that epitomises the microanalytical approach used for the study and interpretation associated with the production technology, the raw materials used and the mineralogical changes that occur during glazing and firing. With the benefit of current high precision SEM-EDX instrumentation (Goldstein *et al.* 2003; 2018) it is timely to be reminded of the early paper by Freestone (1982), *Applications and potential of Electron Probe Micro-Analysis in technological and provenance investigations of ancient ceramics*, for which we hope this paper is complimentary to that early foresight.

In this paper, we illustrate the use of high-resolution X-ray compositional mapping (*ca.* 4100x2900 pixels) and associated backscattered electron (BSE) compositional images on one typical thick section of this type of complex microstructural glazed ceramic. The sample consisted of a polished section of a sherd (TW01⁴) from an early 16th century Italian maiolica plate (glaze and body) from Faenza with cobalt blue *berettino* decoration, similar to the sherd (sherd 5) shown in Figure 1 (lower).

Preliminary analytical data for the sherd (TW01) had previously been included in recent papers on the production technology of Italian maiolica (Tite 2009; 2012).

EXPERIMENTAL PROCEDURES

The maiolica sherd sample was mounted in cold-setting resin block 30mm diameter and 10mm deep and diamond polished to a very high finish, and optical micrographs taken (Figure 2a-c).



Figure 2a. Optical microscopy of the polished maiolica sample in the resin block.

⁴ Professor Tim Wilson (ex-Ashmolean Museum) is thanked for providing sherd TW01.

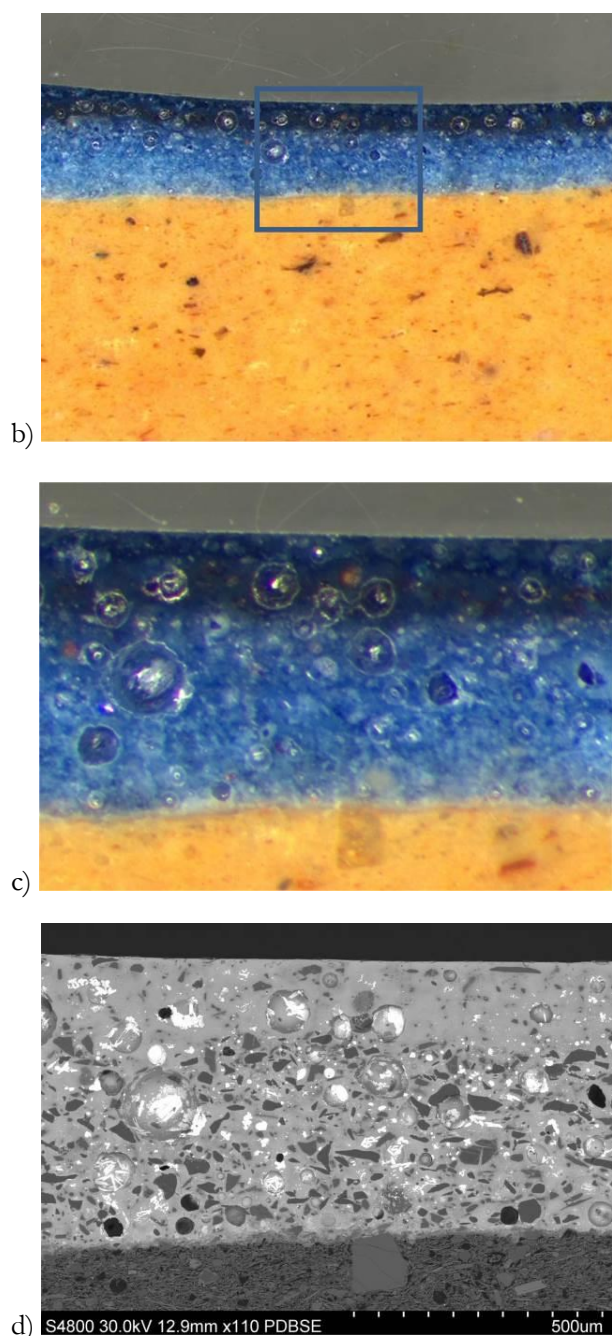


Figure 2 b), c). Optical microscopy of the polished maiolica sample in the resin block. Note the two layers of the blue glaze - the upper transparent deeper blue glaze and lower opaque glaze which appears lighter in colour due to tin oxide opacifier crystals. d) BSE image of the SEM-EDX map area showing the very complex mineralogy within the glazing.

The sample was vacuum coated with an extremely thin conducting layer of carbon for study in the high vacuum high-resolution SEM. The coating is not seen in the SEM under the operating conditions used.

The high-resolution study was carried out using an Oxford Instruments AZtec® EDX microanalysis

system⁵ run on an Hitachi S-4800FE field emission scanning electron microscope (FE-SEM) at the British Museum (London, United Kingdom). This combination provided two advantages - the very high-resolution digital X-ray mapping provided by the AZtec® microanalyser, *ca.* 4100 x 2900 pixels, combined with the high-resolution imaging capability of the FE-SEM at high magnification (Goldstein *et al.* 2017; Lyman *et al.* 1990). For imaging and analysis, the FE-SEM was run at 20kV which provided the best backscattered electron imaging for high contrast and low noise of the complex mineral and glassy phases in the ceramic sample (Meeks 1988). This is also the best kV to energise the full range of elements of interest for EDX analysis (Russ 2013, Statham 1998) of this maiolica, from the lighter ceramic matrix elements (O, Na, Mg, Al, Si, K, Ca), through the transition elements (Ti, Mn, Fe, Co, Ni) and up to the useful diagnostic high energy element lines of lead/arsenic/bismuth (*ca.* 10.5-13keV) on a spectrum range 0-20keV (Kortright and Thompson 2001⁶). The conditions provide efficient spectral collection at high count rate (*ca.* 9000cps with the particular analyser used) for X-ray elemental mapping and analysis. With such a large digital map image, *ca.* 12 million map points, for which a full spectrum is obtained from each point, the time required for mapping is necessarily long, typically (overnight) for 16 hours, and the digital storage required is large (e.g. can be in the gigabyte range). The resulting map contains all elements of interest in the sum spectrum for the whole mapped area from which any, or all, detectable elements can be selected for reconstructing into elemental distribution maps.

The high-resolution BSE image of the mapped area allows very useful digital zoom for more detailed investigation of the complex microstructures, mineralogy and chemistry, without pixelation of the image or maps (see Figure 11). Selected areas can be made within the mapped area, for example on a high concentration element in an inclusion of interest, in which the associated pixel spectra are combined into a summed spectrum for that area which can be quantified.

RESULTS AND DISCUSSION

Body of the maiolica sample

The EDX analyses by Tite (2009, tables 1 and 3) of the ceramic body bulk composition (paste) of a number of Italian maiolica sherds include sample TW01. This sample is examined in detail here, as it is

⁵ See Oxford Instruments Nanoanalysis *Application Notes*.

⁶ See *X-ray Emission Energies*.

a typical of Italian maiolica of the Renaissance period.

The investigation here gives analyses of a typical body (paste) area mapped at $\times 400$ (ca. $320 \times 220 \mu\text{m}$ area) with mineral inclusions, typically ranging between $15\text{--}70 \mu\text{m}$ across or in length, set in a fine network of interconnecting relict clay/glass phases (Figure 3). The microstructure, observed by backscattered electron imaging shows the mineral distribution, and the EDX-maps highlight the elemental concentration of the minerals (Figure 4a and b) and the quantitative analyses of these minerals provides their likely identification from the major element proportions present and the consistency with which these analyses occur on different analysed grains within an area (Figure 5). Combining the results of BSE compositional imaging, element distribution maps and quantitative analyses, the maiolica sample body consisted predominantly of quartz, feldspars, chlorite, mica and other less abundant mineral inclusions, such as pyroxene (Figures 3 and 5). FE-SEM high resolution imaging at increasing magnification of the body (paste) of the

maiolica can be seen in Figure 3 ($\times 400 - \times 10000$) displaying increasing detail of the interstitial fired clay particles, the range of mineral grains, and the interaction zones and glassy phases of the matrix fusing the particles together.

Elemental mapping

On the basis of the compositional maps for Si, Al, Na, K, Ca, Mg, and Fe (and O) (Figure 4a) together with the quantitative analyses of selected mineral inclusions within that area (Figure 5, Table 1), the rounded quartz grains, were readily identified by the Si map, in which they are visible as white on red areas and also by being absent from all the other maps (dark areas). Rounded potassium feldspar grains were identified from the Si, Al and K maps (Figure 4a) in which they are visible as colour concentrations co-existing (overlapping) the same mineral areas. Similarly, the much rarer, rounded sodium feldspar grains are visible, in particular) as one larger grain in the Na, Si, Al maps. In a different map area (Figure 4b), there are a number of surviving longer acicular particles having the layered morphology characteristic

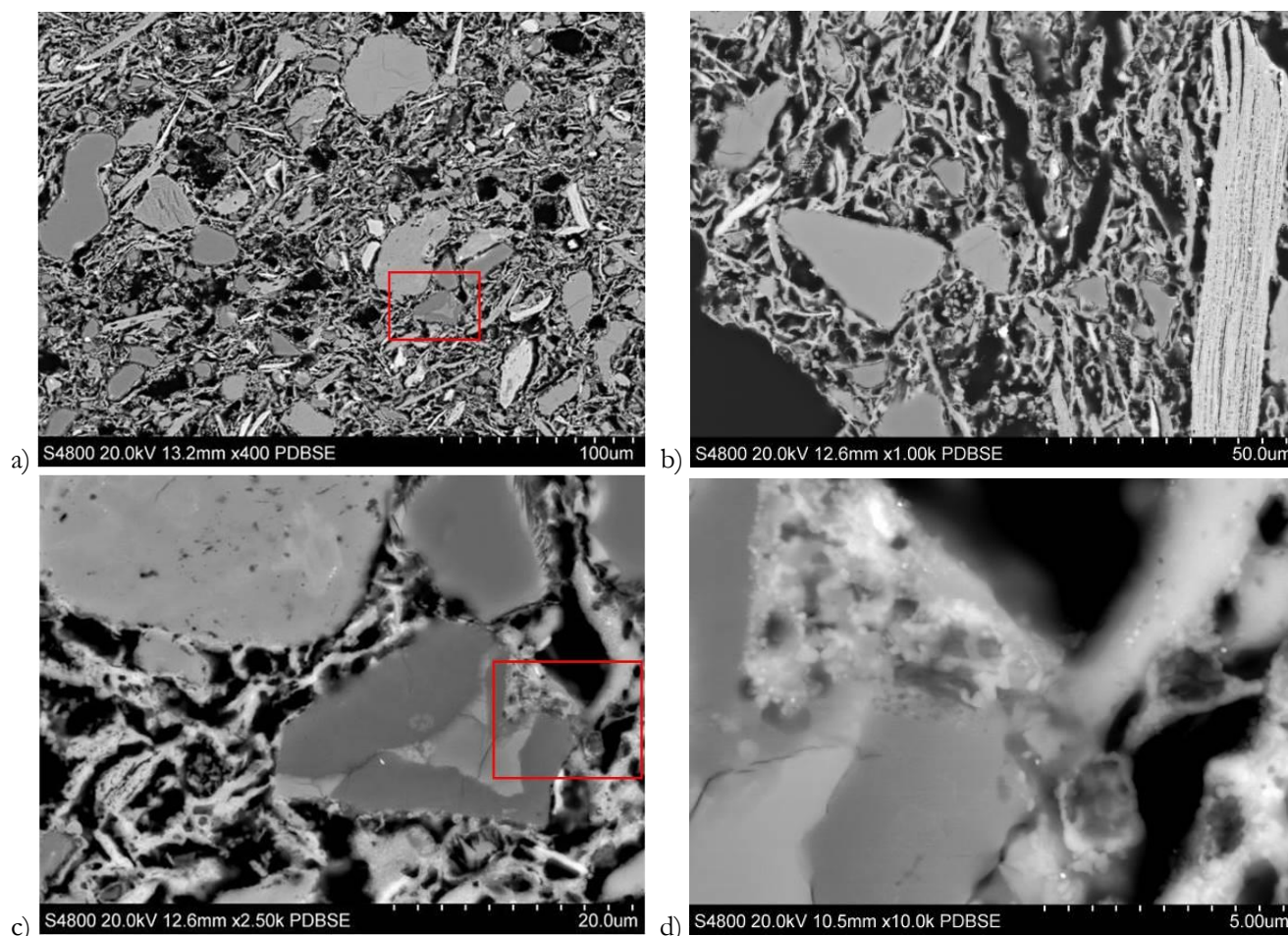


Figure 3. Maiolica sample TW01 paste at increasing magnifications a) $\times 400$, b) $\times 1000$, c) $\times 2500$, d) $\times 10000$, showing the mineral grains, layered mica (b), and the glassy filaments binding minerals in the fired clay matrix (d).

of mica, which is confirmed by the correlation between Mg, K and Fe (Figure 3b and map Figures 4a and 4b). In addition, within the area of the polished section illustrated in Figure 5, there is a single, slightly triangular, pyroxene (clino-enstatite) grain which is visible as the large white on red grain in the Mg map, and as a corresponding pale green-blue grain in the Si map (Figure 4a and Figure 5 -

Table 1 spectrum 3). Table 1 comprises quantitative analyses of the bulk composition and a number of the more prominent and smaller mineral grains in the ceramic body mapped area, and Figure 6 illustrates typical spectra from Table 1 representing specific minerals present by showing their characteristic elemental signatures.

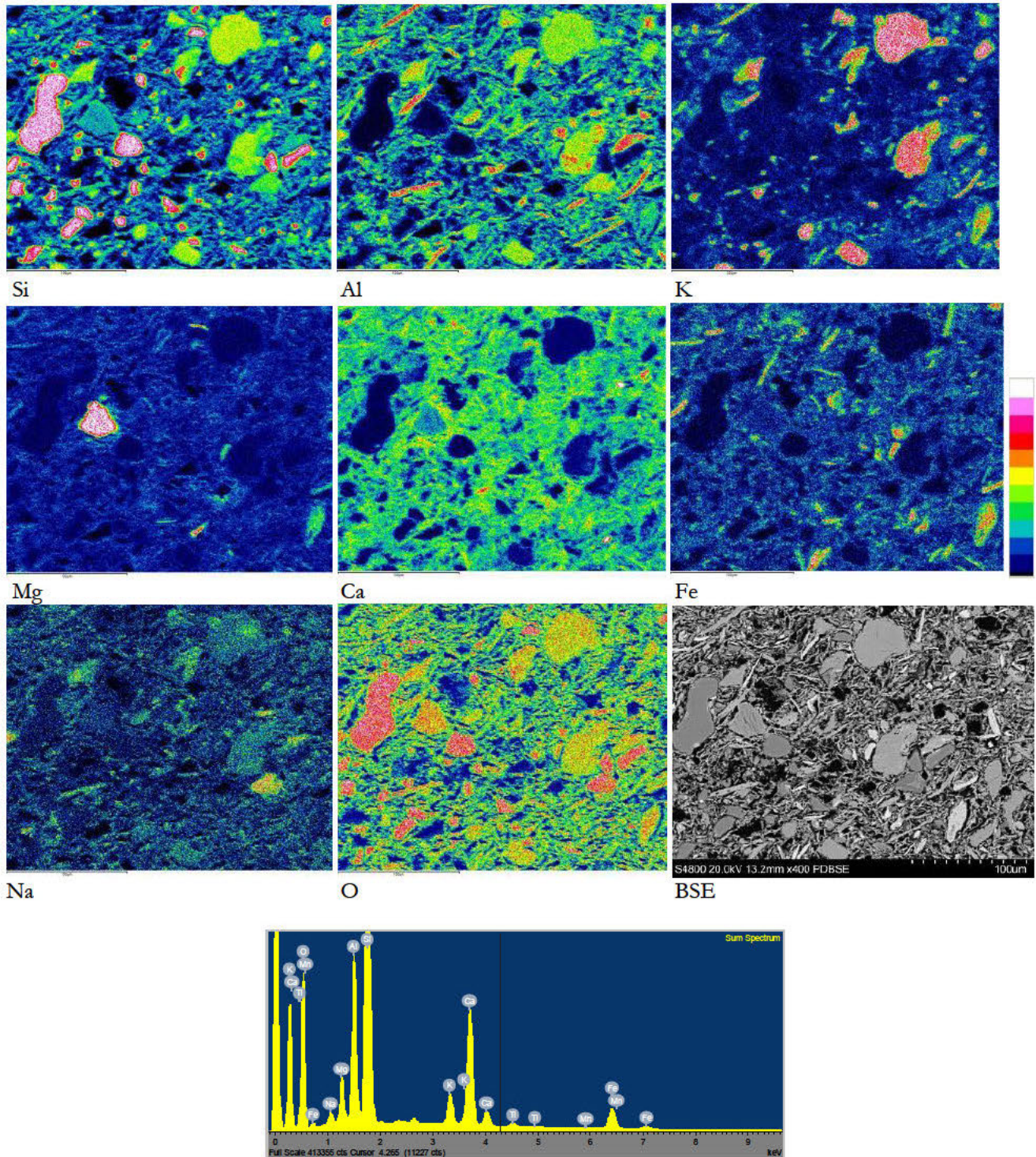


Figure 4a. EDX element maps ($\times 400$, width of image $300\mu\text{m}$) showing relative element concentrations between minerals and paste. Note the uniformly distributed calcareous paste and overall oxide (oxygen) concentrations, whereas few calcitic mineral grains appear in the paste map. Bottom: map area sum spectrum of the paste, with high calcium peak denoting the overall distribution in the paste area.

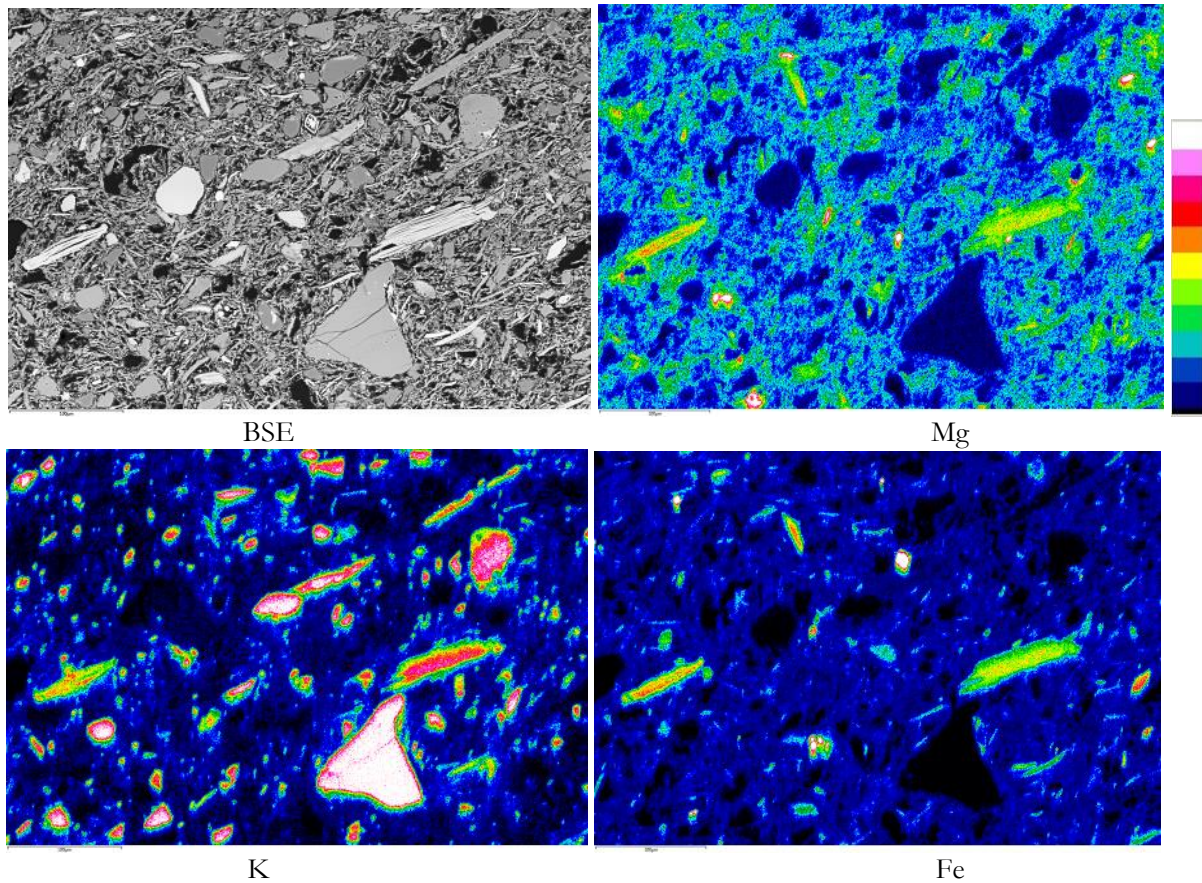


Figure 4b. TW01: element maps (x240) of a different area of the maiolica paste, showing correlation of Mg with K and Fe in the laminated shape characteristic of biotite mica.

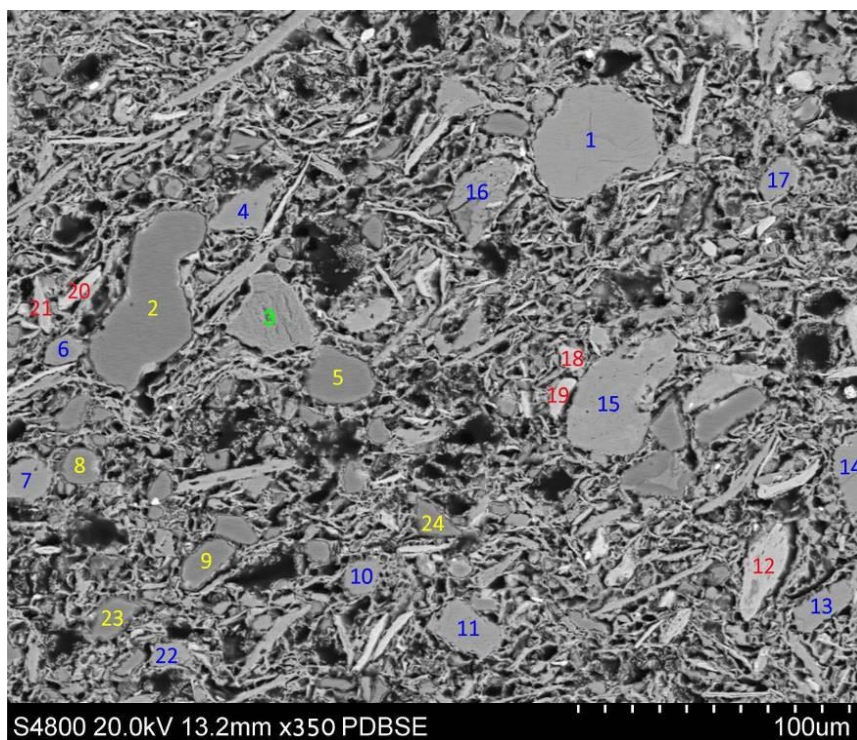
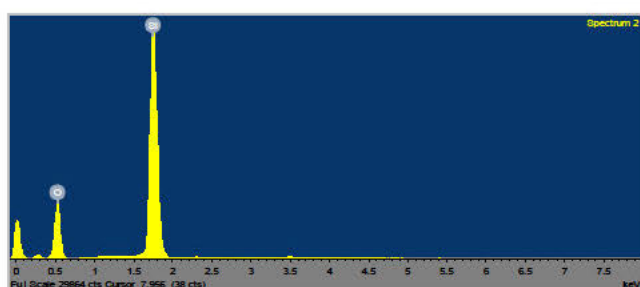


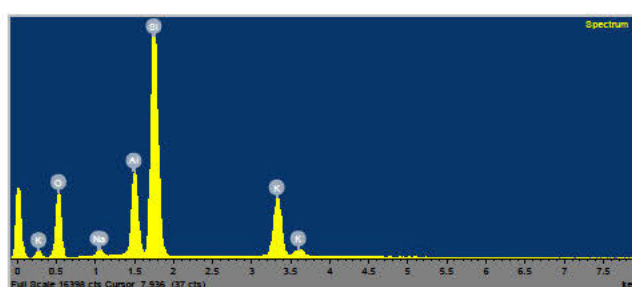
Figure 5. Sample TW01: BSE image of the mapped area with individual spot analyses of the minerals. Note the grey level differences in the BSE image between different mineral types. There are two principal mineral groups and two less common minerals in the paste; legend: quartz Si; feldspar: K, Si, Al; chlorite group: Mg, Si, Fe, Al, K, Ca; Pyroxine/Clino- enstatite Mg, Si, Ca grain (see also Table 5 below).

Table 1: TW01, paste area map: typical analysed minerals with their spectra, see Figure 5.

Mineral Spectra	wt% oxides									
	Na	Mg	Al	Si	K	Ca	Ti	Mn	Fe	
Spectrum 2	0.0	0.0	0.0	100.0	0.0	0.0	0.0	0.0	0.1	
Spectrum 3	0.2	41.9	1.6	46.3	0.3	7.4	0.1	0.1	2.6	
Spectrum 15	1.8	0.0	19.2	64.0	13.1	0.9	0.0	0.0	0.3	
Spectrum 20	0.5	9.5	20.3	33.4	5.5	7.6	0.2	0.3	20.4	
Mapped area	1.3	4.4	15.4	56.7	2.8	13.3	0.6	0.13	5.4	



Spectrum 2: Quartz; Si, O



Spectrum 15: Feldspar; Si, Al, K, O

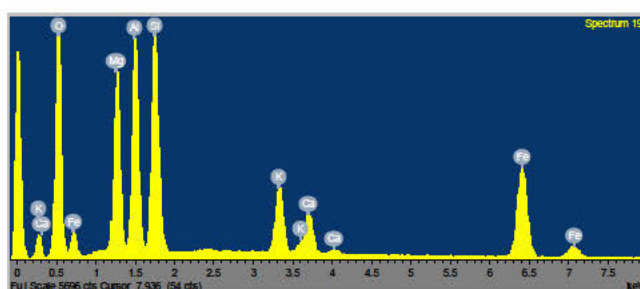
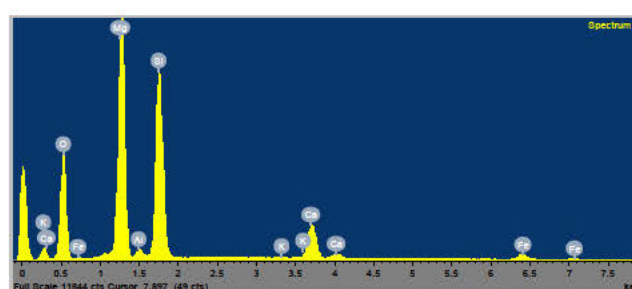
Spectrum 20: Chlorite group
Si, Al, Mg, Fe, O (plus lower K, Ca)Spectrum 3: Pyroxine/clino-enstatite Mg, Si, O,
single grain (plus small Ca, Fe, Al peaks)

Figure 6. Selected spectra from Figure 5 in Table 1.

Apart from a very few, small lime-rich particles (<5 μm across), the lime (CaO) content of the body is homogeneously distributed in the paste within which the other mineral inclusions are embedded and fused together with glassy phases and filaments. Overall, the maps show the interconnecting network consisting of calcium aluminium silicates that have incorporated iron oxide, together with limited amounts of a glass phase, which is associated with presence of soda (Figure 3d). The presence of the iron oxide in the silicates resulted in the characteristic buff colour of calcareous clay bodies, rather than the red colour that would have resulted if the iron oxide had survived as haematite.

Glaze

One of the most striking things about the maiolica plate is the intense deep blue colour of the glaze (Figure 1, which is dramatically seen in the polished cross section in Figure 2). The blue glaze applied to the sherd is *ca.* 600 μm thick (at the point of the

examination) but is seen as two distinct layers, an inner opaque glaze (*ca.* 420 μm thick) corresponding to the *coperta* layer described by Piccolpasso (*ca.* 1557) of a lighter blue colour, and an outer transparent deeper blue glaze (*ca.* 180 μm thick) (Figure 2)⁷. The two optical blue layers are associated with two distinct glaze layers and glazing events, and are due to differences in the chemical and mineralogical compositions from the manufacturing processes. It is at this point that the power of high-resolution FE-SEM-EDX imaging, analysis and X-ray mapping can be applied to discover their microstructure and composition, and hence the materials used in their formation.

The first noticeable impression of the SEM BSE image (Figure 2d) is the complexity and variety of the mineral components within both transparent and opaque glaze layers. The most noticeable difference being that the region of the optically transparent glaze has less large and mineralised inclusions

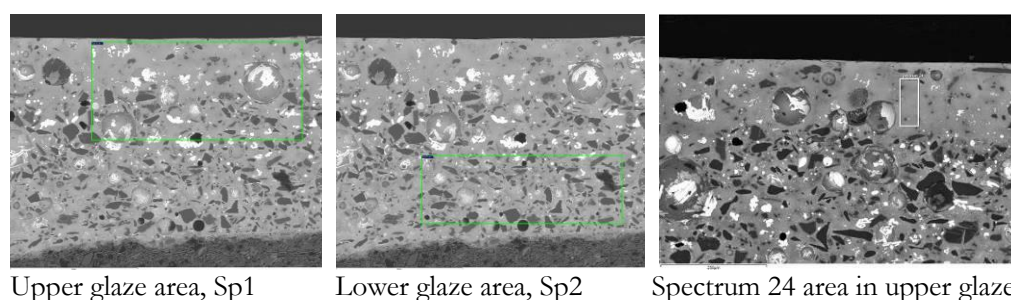
⁷The two-colour layer variation was also noted by Tite (2009).

compared with the underlying optically opaque glaze. Understanding the microstructural complexity was approached from two chemical analytical directions: X-ray mapping of the entire field of view at very high pixel density (4100x2900 pixels) to give the overall chemical viewpoint and distribution of minerals and phases, followed by EDX analysis of key regions, minerals and phases. The combination of the two would provide identification of the minerals added,

the glaze matrix composition and the glaze colourant and hence the processes of manufacture.

Analysis of the glaze layers

General area analyses of the upper and lower glaze layers incorporate all the minerals in the layers as well as the glassy matrix. Both glaze layers are leaded with low soda and the presence of cobalt as the blue colourant and tin oxide as the opacifier in the lower opaque blue glaze (Figure 7, Table 2).



Spectrum wt% oxides	Na	Mg	Al	Si	K	Ca	Ti	Mn	Fe	Co	Ni	As	Sn	Pb
Spectrum 1 upper glaze	1.9	0.5	5.0	61.6	6.1	1.5	0.1	0.0	2.3	2.7	1.4	3.1	2.3	11.4
Spectrum 2 lower glaze	1.5	0.4	5.2	66.9	5.6	1.4	0.1	0.0	0.8	0.8	0.3	1.2	3.9	11.9
Spectrum 24 upper glaze free of mineral inclusions	2.1	0.5	4.7	58.9	6.7	0.9	0.1	0.0	3.4	2.4	0.6	1.3	0.3	13.5

Figure 7 & Table 2. General area analyses of the upper and lower glazes (spectra 1 and 2). Note how the cobalt, nickel and iron values in the different areas correspond well to their relative concentrations in the maps (Figure 15 below). Note also Spectrum 1 clips the lower glaze so that more tin is incorporated - see Sn map. Whereas an area of the upper transparent glaze above the tin oxide opacified lower glaze has much reduced tin, spectrum 24 (see Sn map Figure 12).

EDX high resolution maps of the complex glaze of the polished maiolica sample

EDX maps of the glaze show clearly defined mineral grains with elemental associations combined for specific minerals, and diffusion zones and concentrations within the glaze (Figures 8, 9, 10, 11, 12, 15, 18). Element lines for maps were chosen to avoid overlapped peaks and results checked by EDX analyses, for example Pb and As, Sn and Ca as these are important fingerprint elements in the glaze, and also Co, Ni and Fe as these are associated with the blue colourant and its associated remnant minerals. In addition, potential overlapped X-ray lines such as As 'L' and Mg 'K' can be further interrogated by the feature 'Truemap' within the Oxford Instruments analyser which does complex peak subtractions at overlap regions.

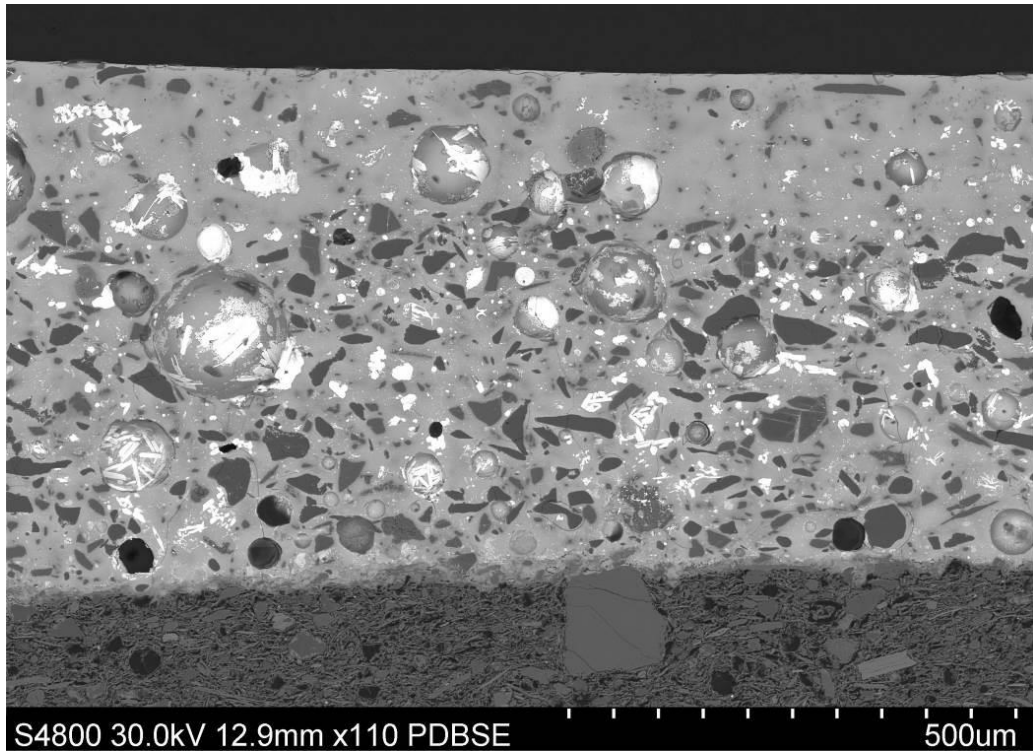
Quartz and feldspars

Quartz grains are clearly identified by the white-coloured mineral concentrations in the Si map distributed mainly within the lower glaze areas (Figure 8). The positions of these angular grains also

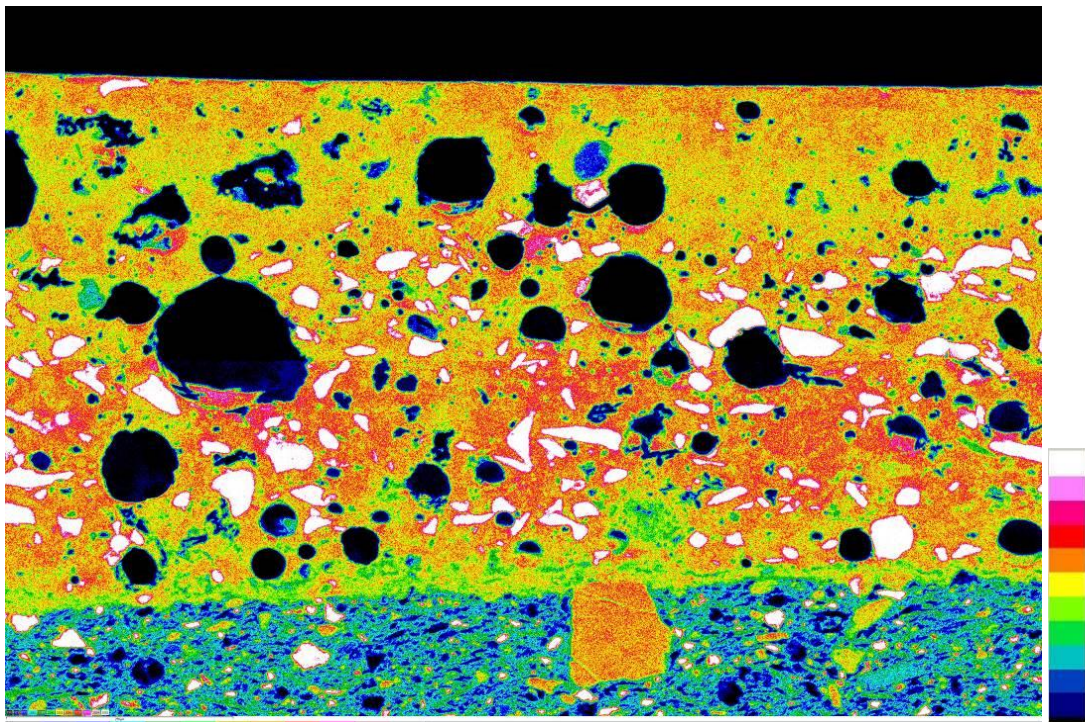
show as corresponding black areas on other maps (e.g. Figure 9, K map). Potassium feldspar grains are identified by the association of Al and K concentrations in the same mineral grains throughout both the outer transparent and inner glaze layers (Figure 9), and are slightly angular and are present in slightly smaller numbers.

Note that the silica contents of the feldspars are similar to those of the dissolved silica in the glaze itself (i.e. some 60 wt% SiO₂). These feldspar grains cannot be seen on the Si map, even as outline shapes, as they merge seamlessly into one uniform silicon concentration distribution (Figure 8). It is therefore important to map each of the main elements and compare all of the maps for correlation within mineral grains.

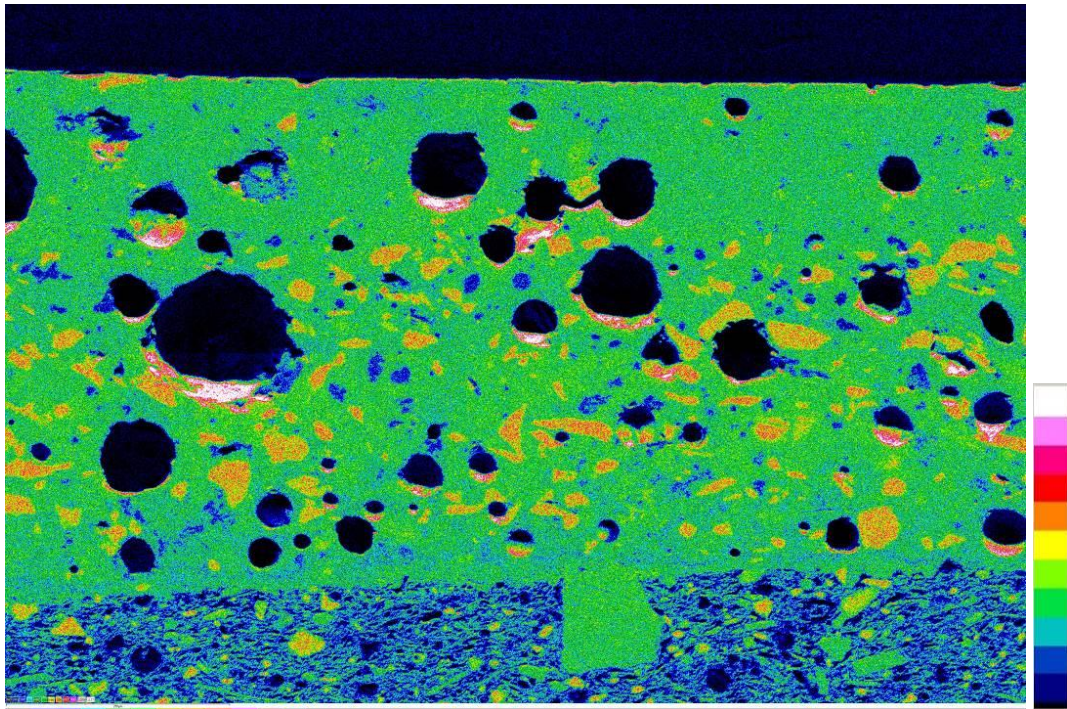
The Na map shows low soda, characteristic of lead-alkali glazes, throughout the glaze layers, but occasional sodium feldspar grains were identified as the cluster of three white grains in the lower glaze, one larger and two smaller adjacent grains (Figures 10 and detail Figure 11).



SEM BSE image

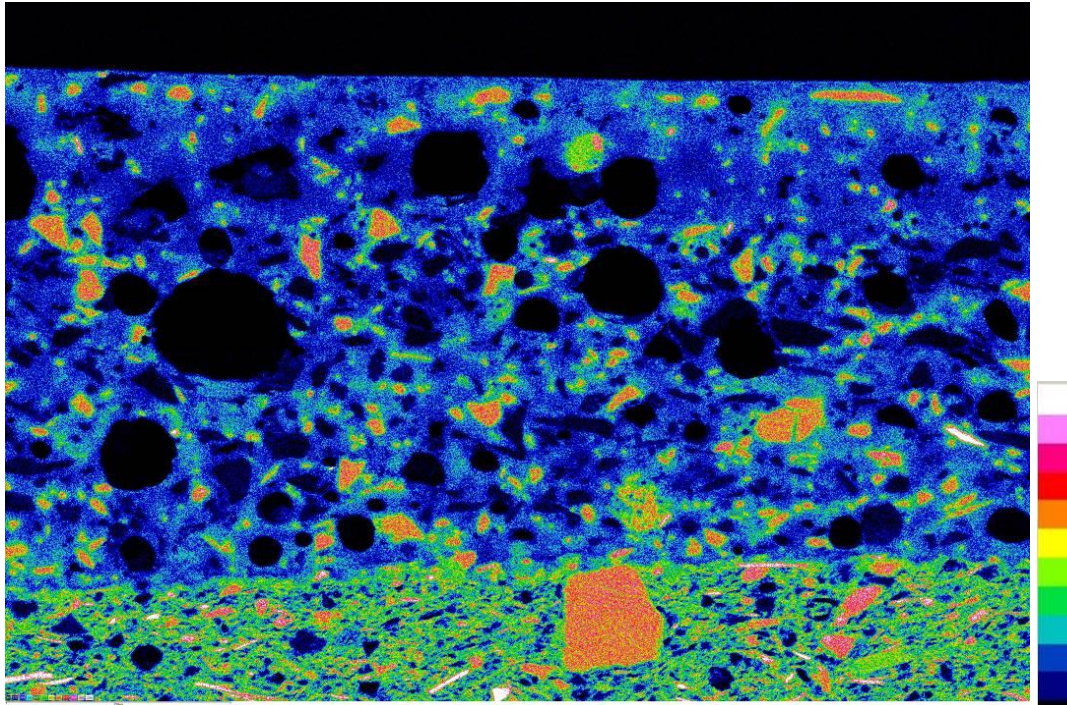


Si 'K' line map. Note the quartz grains are white.

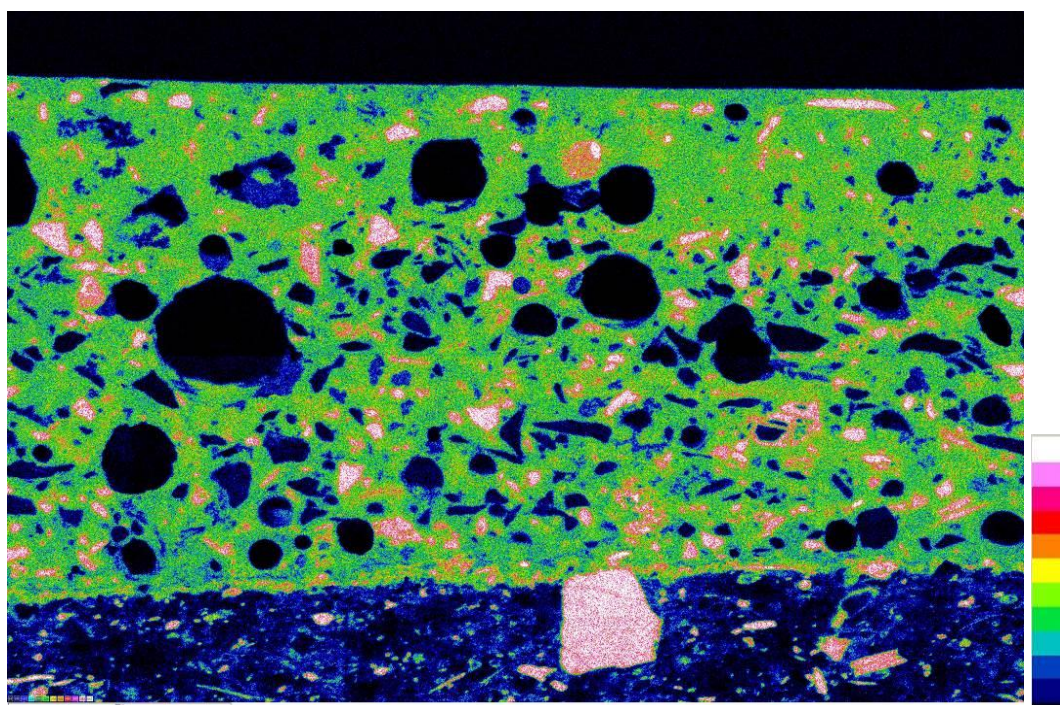


O 'K' line map. Note the quartz grains are orange.

Figure 8. Top, SEM-BSE image of the region examined in detail by SEM-EDX mapping and analysis c. 1x0.8mm area at x110. Note the gas porosity in the glaze shows as round black holes in the maps due to the X-ray detector having low-angle geometry, but the BSE image shows crystalline features in these pores because the electron detector is directly above the area.

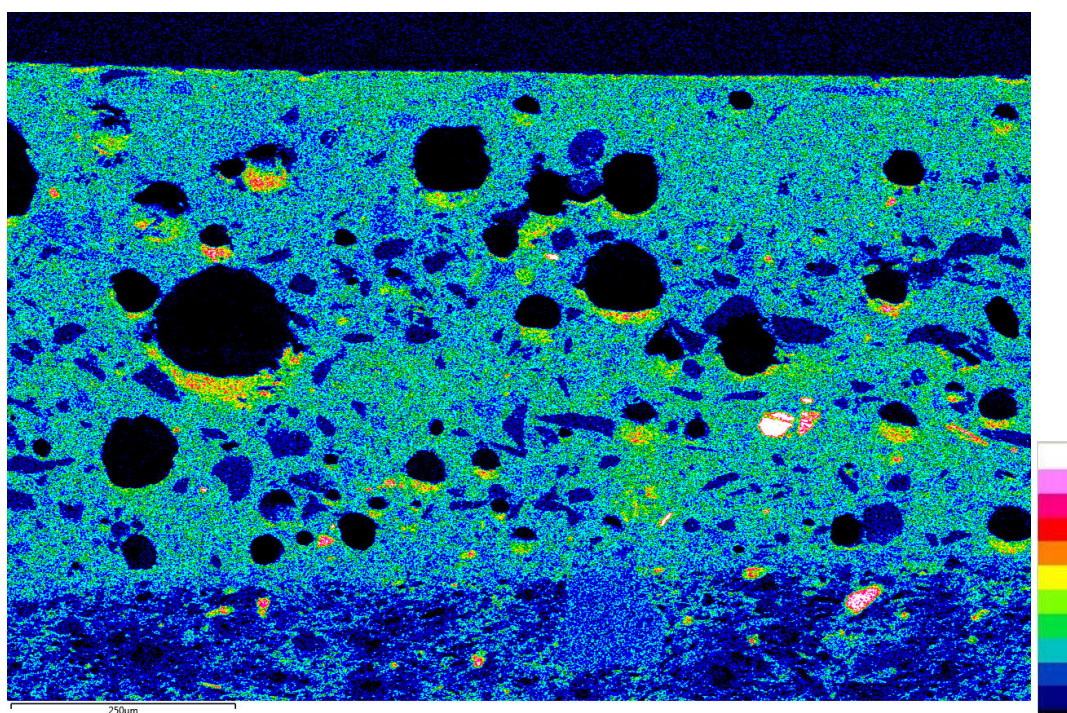


Al 'K' line map. Feldspar grains are orange.



K 'K' line map

Figure 9. Feldspar grains (Al, K silicates): association of concentrations in the Al and K maps. They are throughout the two glaze layers and within the ceramic paste.



Na 'K' line map

Figure 10. TW01, Na map: generally low soda content of the glaze (c 2.1% Table 2 spectrum 24) and ceramic paste. Note the occasional Na feldspar grains (white, and see detail in Figure 11).

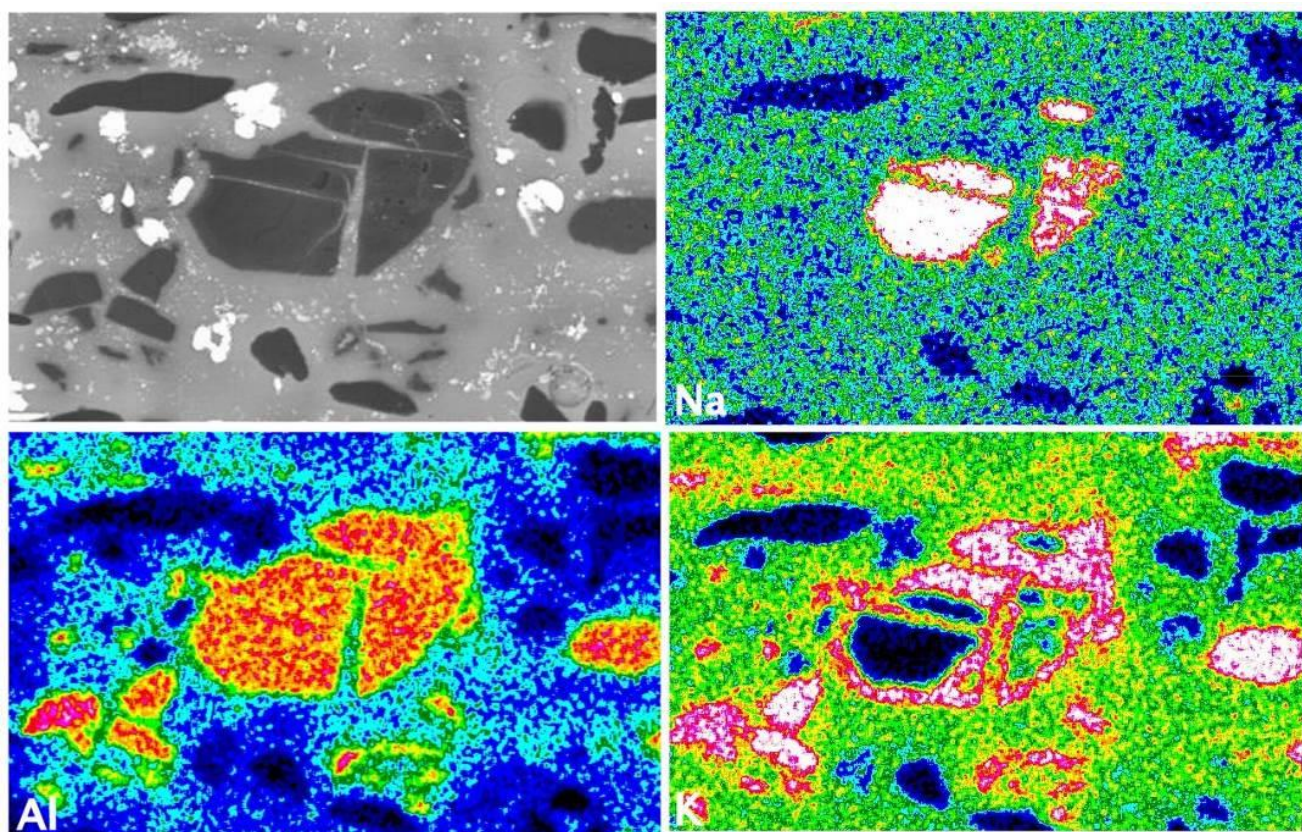


Figure 11. BSE image and selected map area detail of the complex Na/K/Al feldspar mineral grains extracted directly from the full area high resolution maps (Figures 9 and 10). Width of each map 165 μ m.

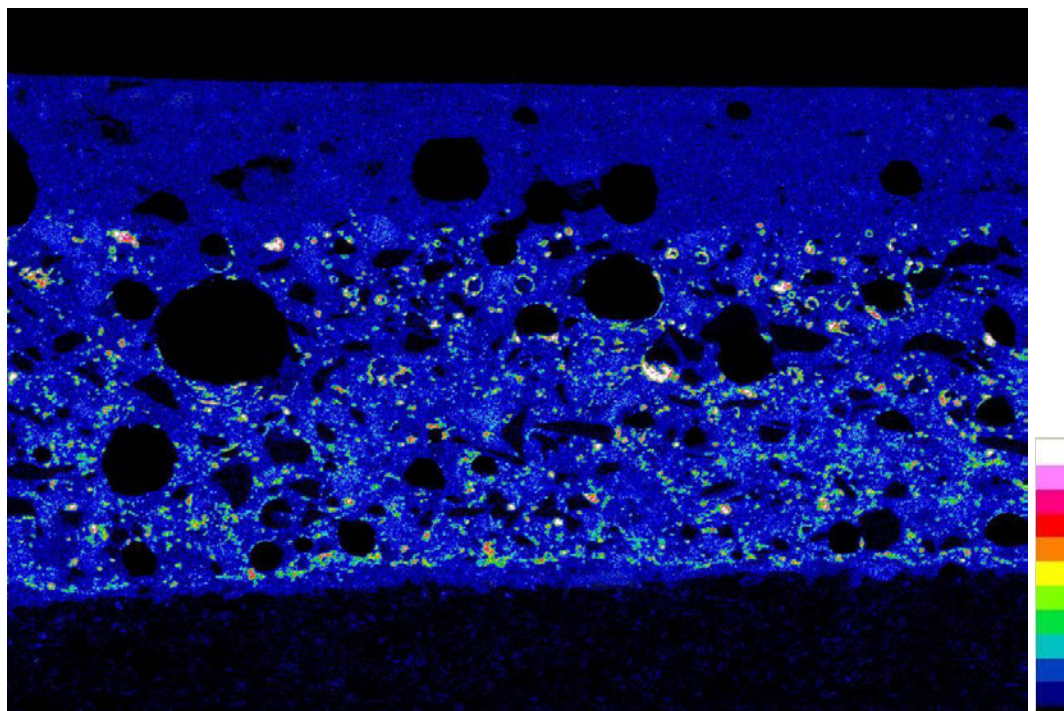
By extracting detail maps from the original high-resolution map, it becomes clear that the feldspar mineral is a fractured grain having a composite Na/K two-phase morphology (Figure 11). This is a good illustration of the way an original 4100x2900 pixel high-resolution map retains all the chemical and morphological information in a single map image and allows digital zoom interrogation retaining a good resolution image. It also illustrates the point to be aware that different chemical phases within a mineral grain can have similar BSE grey level contrast images by having similar mean atomic numbers (Figure 11), and even similar relative levels of a particular element; in this case Al which shows a uniform concentration in the large central grains (red/yellow), and on its own masks the complex mineralogy which is revealed by the Na and K element concentrations seen in different regions within the same grain.

Tin oxide opacifier, inner glaze

The Sn map (Figure 12) shows the inner opaque glaze layer (ca. 420 μ m in thickness) has a fairly uniform distribution of mainly fine tin oxide particles, present as individual small acicular particles about 1-2 μ m long. These are absent in the outer glaze layer. In addition, tin oxide is sometimes

present as clumps up to ca. 30 μ m across (Figure 13 and image in Table 3), whereas others are much smaller and seen at 20,000x magnification, as individual acicular sub-micron crystals, ca. 0.44x0.1 microns in size, some of which appear to show some microscopic crystal orientation in the glass (Figure 14a-c). Molera *et al.* (1999) also show medieval tin glaze has a particle size of tin oxide of around several hundred nanometers, which corresponds to the range of wavelength of visible light. They also noted that in some cases, the tin oxide is presented not only as small crystals but also as aggregates of particles. These factors – the high refractive index, the low solubility in glazes and the particle size make tin oxide an excellent opacifier.

This inner glaze also has a distribution of quartz particles up to about 80 μ m across, and fewer feldspar particles up to about 50 μ m across which result from the addition of sand to the fritted glazing mixture (Figures 8 and 9, Si, Al, K maps, and also analysed minerals - quartz spectra 13-15 & 17 and feldspar spectrum 16, Figure 19 and Table 6b).



Sn 'L' line map

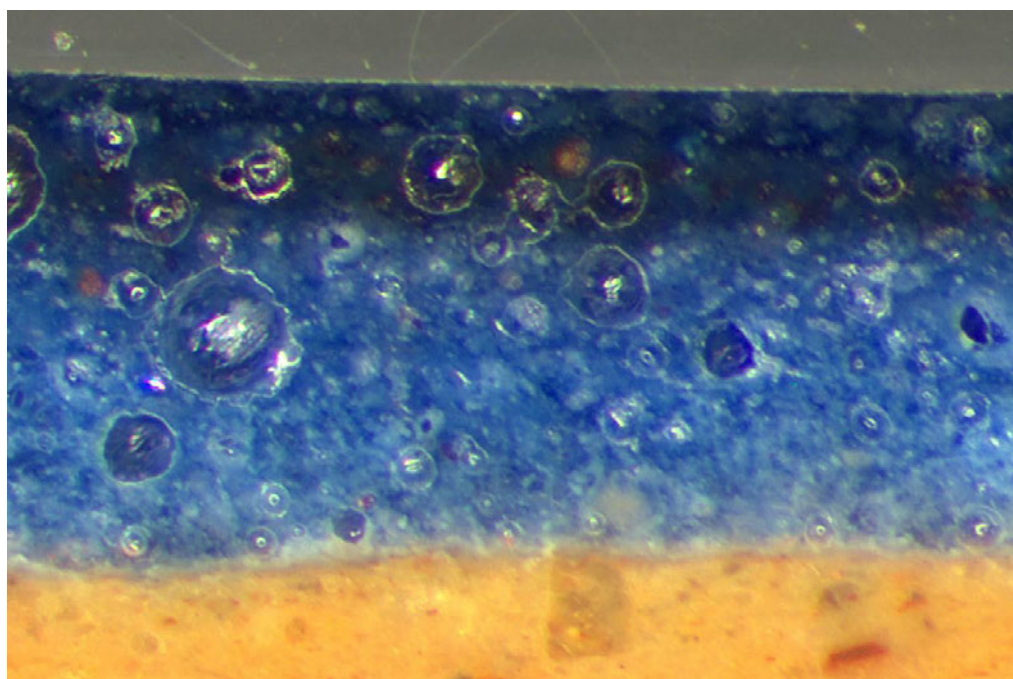


Figure 12. TW01: Sn map (top image) showing tin (oxide) concentrated in the inner glaze as bright particulates, which corresponds to the opacified lighter blue lower glaze in the optical image (also Figure 2). There are no tin (oxide) particles in the upper transparent glaze.

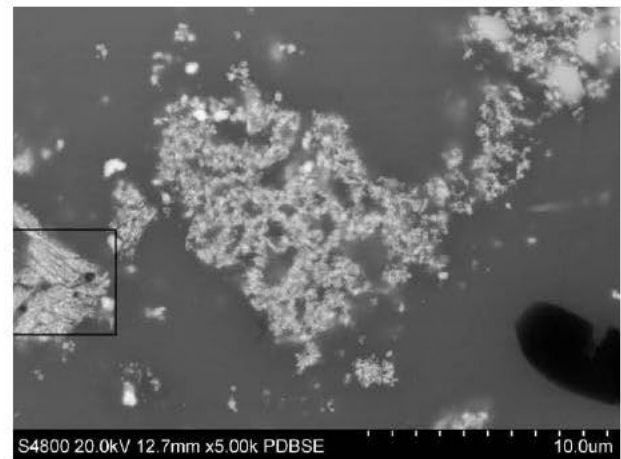
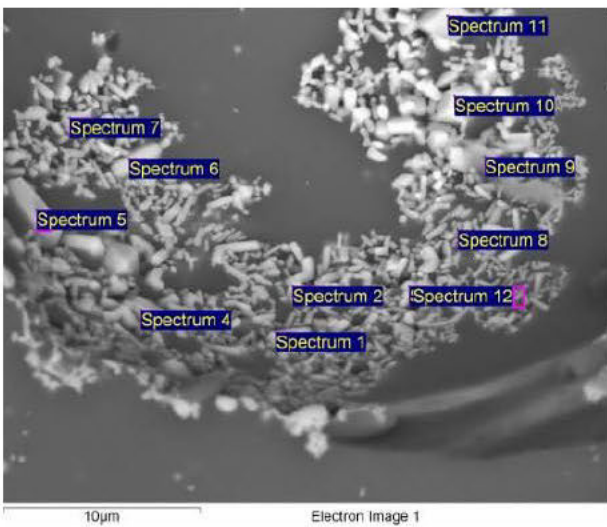
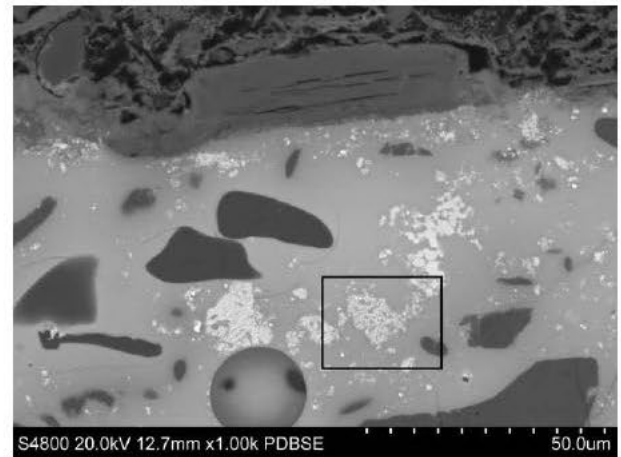
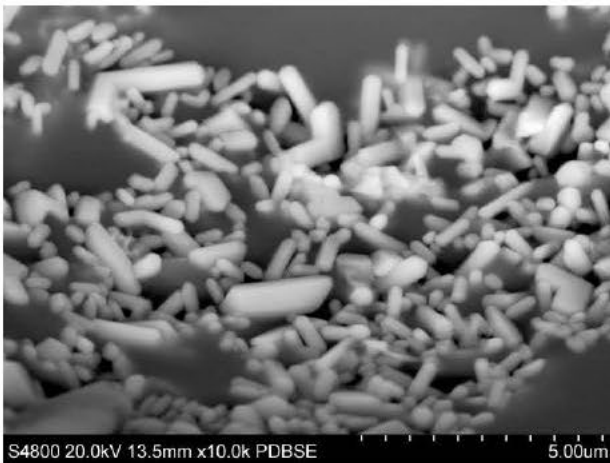
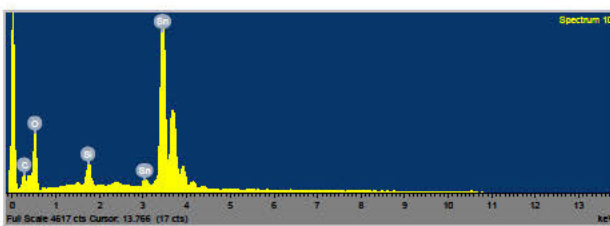


Figure 13. Upper: Tin oxide crystals precipitated in the glaze at the surface of a gas bubble ($\times 10,000$). Lower: point analyses on crystals. See Table 3 below.



Spectrum wt% oxides	Sn	Si	Pb
Spectrum 4	88.5	7.5	1.2
Spectrum 10	90.0	6.9	1.3

Table 3. Spectrum 10: typical spectrum of a larger tin oxide crystals seen in the surface of a gas bubble. Key elements Sn, Si, Pb in their relative concentration selected from analyses (spectra 4 and 10). Note, the Si and Pb contributions are from beam penetration through the tiny crystals of tin oxide and scatter from the glass matrix below. The spectra with highest tin show less scatter (i.e. the largest crystals Spectrum 10, compared with 4).

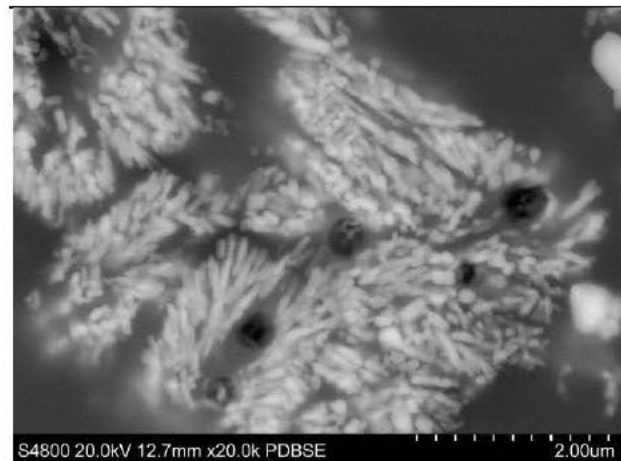


Figure 14. TW01, tin-rich particles at $\times 1000$, $\times 5,000$ and $\times 20,000$ magnification. The white-coloured tin oxide particles that form in the blue glaze are the opacifiers to make it appear opaque and intensely blue. The individual acicular crystals are ca. 0.45×0.1 microns in size.

Outer glaze

In contrast, the outer transparent glaze layer (ca. 250 μm in thickness), which corresponds to the *coperta* layer described by Piccolpasso, was more or less clear of quartz and tin oxide particles (Figures 8 and 12) but contains feldspar grains (Figure 10, maps for K and Al). This two-layer glaze type contrasts with a

single opaque glaze layer, which was also widely used in the production of Italian maiolica ceramics during the Renaissance period. Further, both glaze layers applied to sherd TW01 were of the lead-alkali type (Tite *et al.* 1998) containing around 13.5 wt% PbO and some 8.8 wt% total alkali (Na₂O + K₂O) (Table 2 spectrum 24). The silica content dissolved in the glass phase of the outer glaze was slightly lower than that of the inner glaze, and without quartz gains (see map Figure 8 for relative Si concentrations). This would help to reduce the melting point of the outer glaze that was added in a second process.

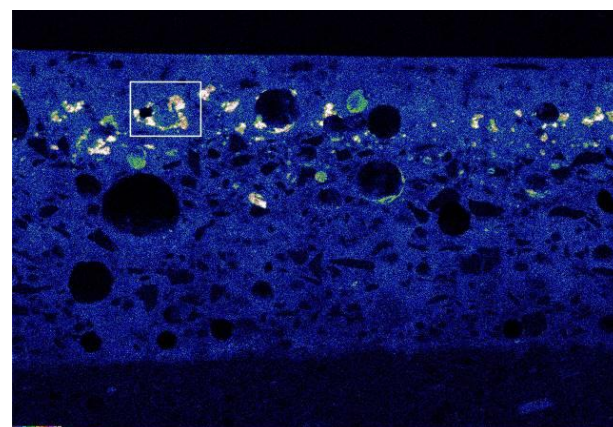
In addition to compositional glaze maps for Si, Al, Na, K, Ca and Fe, equivalent to those for the body of the sherd, additional elements present in the glaze layers were also obtained: Sn, Co, Ni, Pb, As (Figures 12, 15, 18), together with quantitative analyses for selected areas and phases (Tables 2, 3, 4, 5, 6). The Sn map provided a clear demarcation between the opaque inner glaze containing abundant tin oxide particles (map Figure 12) which are visible as small bright precipitated areas in the optical micrograph (Figure 2), but tin oxide particles are absent from the transparent outer glaze.

Cobalt colourant and remnant minerals

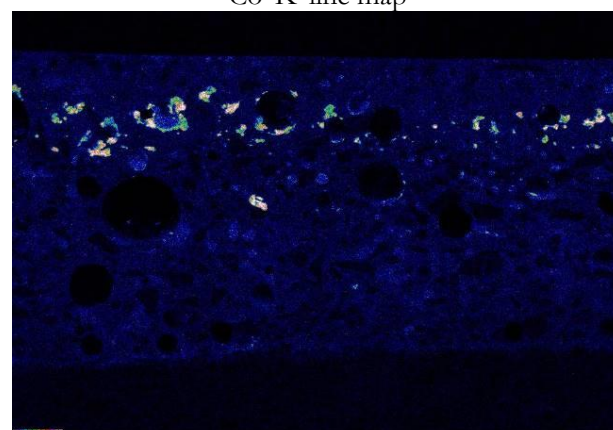
The striking blue colour of the glaze is seen in the sample cross section, Figure 2. Cobalt is dissolved throughout both glazes and is the blue colourant for this glass. The element maps of this section clearly define the association of cobalt (Co), nickel (Ni), and iron (Fe) in a band of remnant mineral particles above the lower glaze layer (Figure 15).

These remnant particles of the cobalt pigment are clearly visible as concentrated bright mineral areas in a distinct broad band at the interface between the two glaze layers on the Co map. It appears that the cobalt-rich mineral grains were applied to the surface of the inner opaque glaze before the application and firing of the transparent outer glaze. Cobalt had diffused during firing throughout the thickness of the outer transparent glaze (*ca.* 2.4 wt% bulk CoO), the colour of which is dark blue; the cobalt also diffused into the opaque inner glaze (*ca.* 0.8 wt% bulk CoO, Table 2), the colour of which is a paler blue. The colour difference is partly due to the lower concentration in cobalt in the inner glaze but also due to the presence of the white coloured tin oxide opacifier crystals already in the underlying first glaze layer. Note that the cobalt dissolved in the glass adjacent to the mineral complex (Figure 16 spectrum 5) is higher than the overall glaze levels due to the dissolution from the nearby cobalt-containing mineral grains. The Ni map matches almost exactly that of the cobalt map, indicating that nickel was

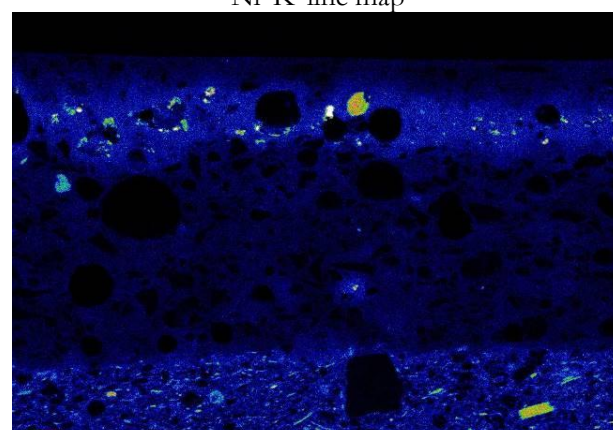
introduced with the cobalt pigment (Figure 15), while Figure 16 and associated Table 5 show some primary cobalt/nickel silicate mineral grains (highlighted orange spectra 3, 4, 7, 8).



Co 'K' line map



Ni 'K' line map



Fe 'K' line map

Figure 15. TW01: cobalt and nickel are in association with each other in remnant minerals containing the cobalt for the blue glaze colouring. Note the Cobalt has diffused throughout the two glaze layers and iron predominantly only within the band in the outer transparent glaze (and is also seen as a constituent of the pottery paste). Square in Co map is the detail area in Figure 16.

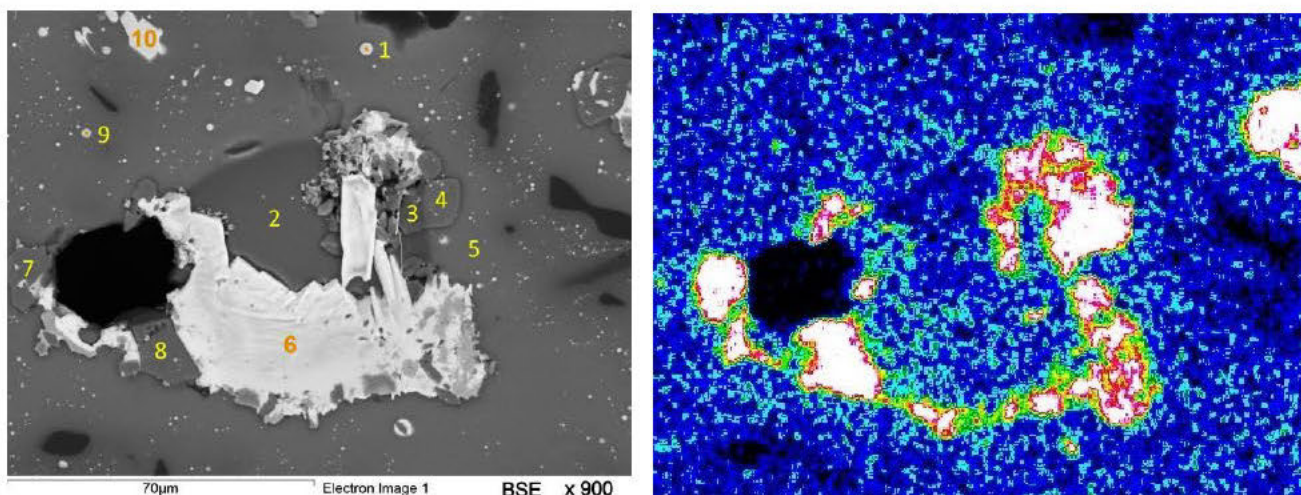
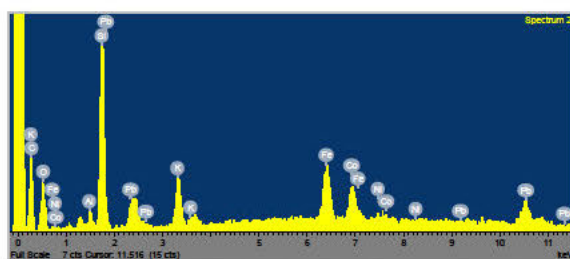


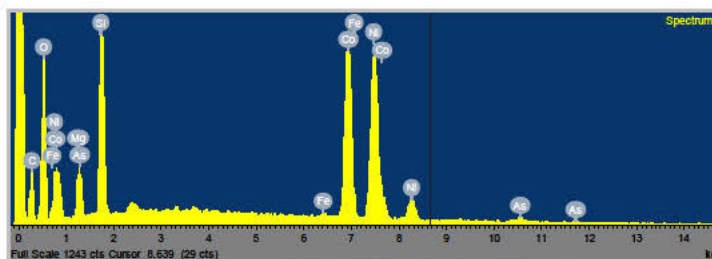
Figure 16. TW01, mineral complex in cobalt-rich area located in the outlined oblong area in the Co map Figure 15 from which the map detail area is taken from this original high resolution map. Note how the Co map clearly shows the individual analysed high-Co/Ni grains, spectra 3, 4, 7, 8 around the large Pb/As mineral grain spectrum 6.

Table 5. TW01, Analysis of complex mineral group in the glaze of Figure 16. Spectra associated with cobalt minerals (main elements - orange and green) and calcium-lead arsenate mineral grains (main elements - blue) (See also Table 6a). Purple is in the glaze area.

Spectrum	Na	Mg	Al	Si	K	Ca	Ti	Mn	Fe	Co	Ni	As	Sn	Pb	Total
wt% Oxides															
Spectrum 1	2.3	0.4	0.7	15.8	1.7	9.5	0.1	0.2	0.9	5.9	2.4	24.6	0.2	35.3	100.0
Spectrum 2	1.0	0.3	2.3	38.1	6.9	0.9	0.1	0.0	21.4	14.9	2.5	2.7	0.6	8.6	100.0
Spectrum 3	0.1	3.9	0.0	19.4	0.2	0.2	0.0	0.1	0.5	33.4	37.6	3.4	0.2	1.2	100.0
Spectrum 4	0.0	1.2	0.1	27.7	0.0	0.1	0.0	0.0	1.0	30.0	38.0	1.3	0.1	0.7	100.0
Spectrum 5 glaze	1.8	0.4	3.2	62.9	7.0	0.7	0.1	0.0	4.9	3.0	0.5	1.4	0.8	13.4	100.0
Spectrum 6	2.9	0.0	0.1	1.9	0.6	11.9	0.0	0.0	0.4	1.2	1.2	34.9	0.0	45.3	100.0
Spectrum 7	0.1	4.3	0.1	28.7	0.1	0.2	0.0	0.0	1.4	28.6	34.6	0.9	0.4	0.7	100.0
Spectrum 8	0.0	4.5	0.0	30.9	0.1	0.1	0.1	0.0	0.4	28.3	33.2	2.1	0.0	0.4	100.0
Spectrum 9	2.5	0.5	1.1	17.4	2.0	8.3	0.1	0.1	1.1	6.1	2.1	25.4	0.2	33.0	100.0
Spectrum 10	1.1	0.0	0.1	1.7	0.7	20.6	0.0	0.1	0.3	0.7	0.0	29.7	0.8	44.5	100.0



Spectrum 2. Fe, Co, Ni, silicate mineral

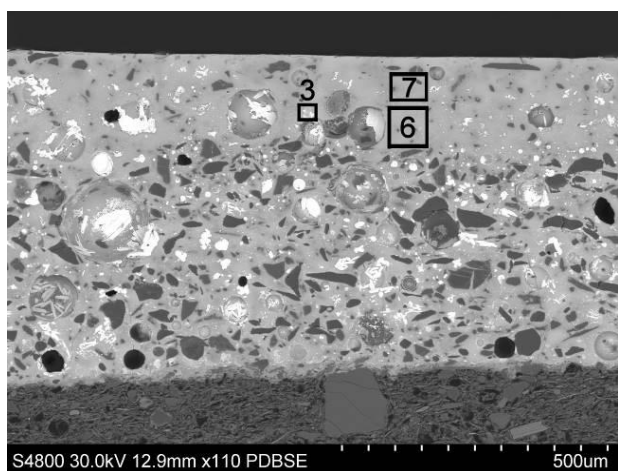


Spectrum 3. Co, Ni, silicate mineral

Iron association with remnant minerals

There is also a general associated matching between the iron map (Figure 15) along the same broad band containing the remnant cobalt/nickel particles in the transparent blue glaze. Some concentrations of iron are found in minerals (brightest regions in Figure 15) that are seen directly associated in aggregates with the

cobalt/nickel silicate mineral grains (in Figure 16 and Table 5 spectrum 2). Iron is diffused within this outer glaze from this mineralised band, although not uniformly throughout this glaze layer, as shown in the small area analyses (Figure 17). The iron, which is much less mobile than cobalt, was almost certainly introduced along with the cobalt minerals.



Spectrum	FeO%	CoO%	NiO%
3 mineral	29.4	15.3	9.2
6 glaze	4.5	2.5	0.9
7 glaze	1.6	1.6	0.4

Figure 17. TW01. BSE image of the maiolica glaze and small area analyses; relative Fe, Co, Ni concentrations. Note how the ratio of Co/Ni remains relatively similar in the glaze while the Fe is progressively less concentrated towards the surface away from the broad concentrated particulate mineral band in Figure 15 map.

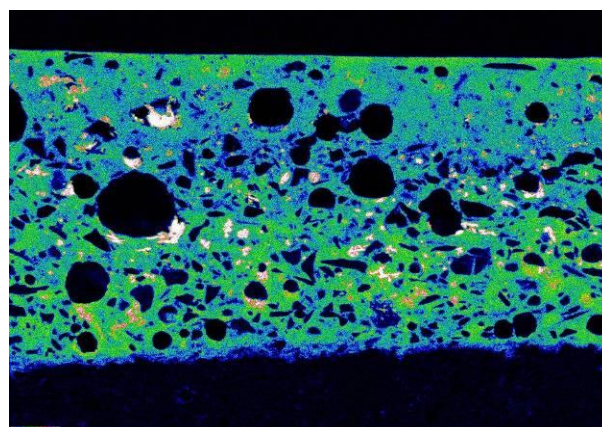
Calcium-lead arsenate crystals

Since arsenic is only present in those Italian maiolica glazes containing cobalt as the colorant, it is certain that the arsenic must have been introduced with the cobalt pigment. As discussed by Zucchiatti *et al.* (2006) and Tite (2009, 2077) the presence of cobalt with arsenic is due to the fact that zaffre is the source of the cobalt colorant which was obtained by roasting arsenic-rich cobalt ore from Saxony in Germany.

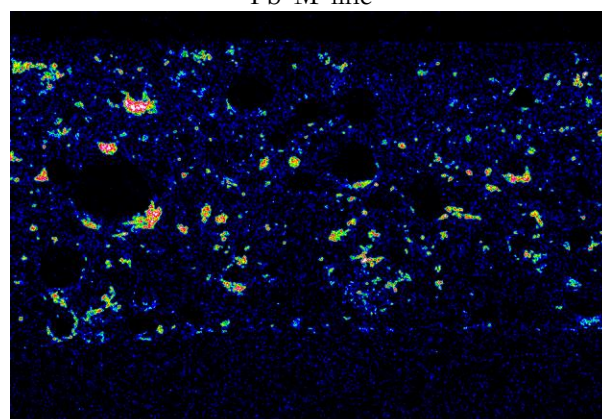
The arsenic map (As 'L') shows that the element appears concentrated in a scatter of complex inclusion areas (up to *ca.* 60 µm across) throughout both glaze layers and perhaps a little more concentrated in the lower opacified glaze layer. Analysis of the glaze between the inclusion areas also shows that during firing, because of its volatility, arsenic is diffused more or less uniformly throughout both the outer transparent and the inner opaque glazes (*ca.* 1.3%, Table 2 spectrum 24).

Looking closely at the distribution of the arsenic, its map concentrations match with areas in both the Pb and Ca maps (Figure 18) which indicates the presence of calcium-lead arsenate particles. These are seen associated with complex minerals found in the general region of the band of high cobalt/nickel/iron minerals. This association is clearly seen in Figure 16 (spectra 6 and 10 in Table 5), with the large

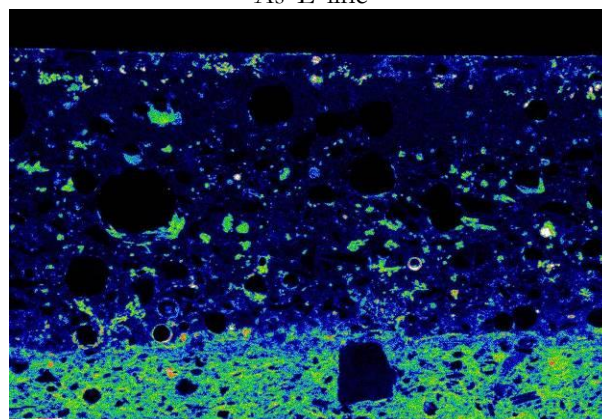
As/Pb/Ca arsenate particles which are in direct physical contact with remnants of the original complex of cobalt minerals Figure 16 (spectra 3, 4, 7, 8).



Pb 'M' line



As 'L' line



Ca 'K' line

Figure 18. TW01: the glaze layers are both leaded. Note the calcareous ceramic paste and the association of Pb, As, Ca minerals in the glaze layers.

However, these particles are not exclusively associated with the remnant cobalt minerals in this band, and are more clearly visible as individual crystals throughout the glaze, see Figure 19 (spectra 1-9 in Table 6a). As previously observed by Zucchiatti *et al.* (2006), the calcium-lead arsenate particles tend to be acicular in shape. These particles

were formed both in random orientation in the glaze matrix itself (Figure 19c), and at the curved surface of gas bubbles in the glaze, where the rather flat acicular form is most clearly seen up to $\approx 30 \mu\text{m}$ in length and up to $5 \mu\text{m}$ across (Figure 19d). It would appear that these characteristically shaped crystals are the reaction product between the diffused As and the

Pb/Ca, which are components of the glaze mixtures, and thus were precipitated from the molten glaze as a by-product of the chemistry of glazing. Some Ca/As/Pb particles are also present as small globules, presumably once molten (Figure 16 spectra 1 and 9).

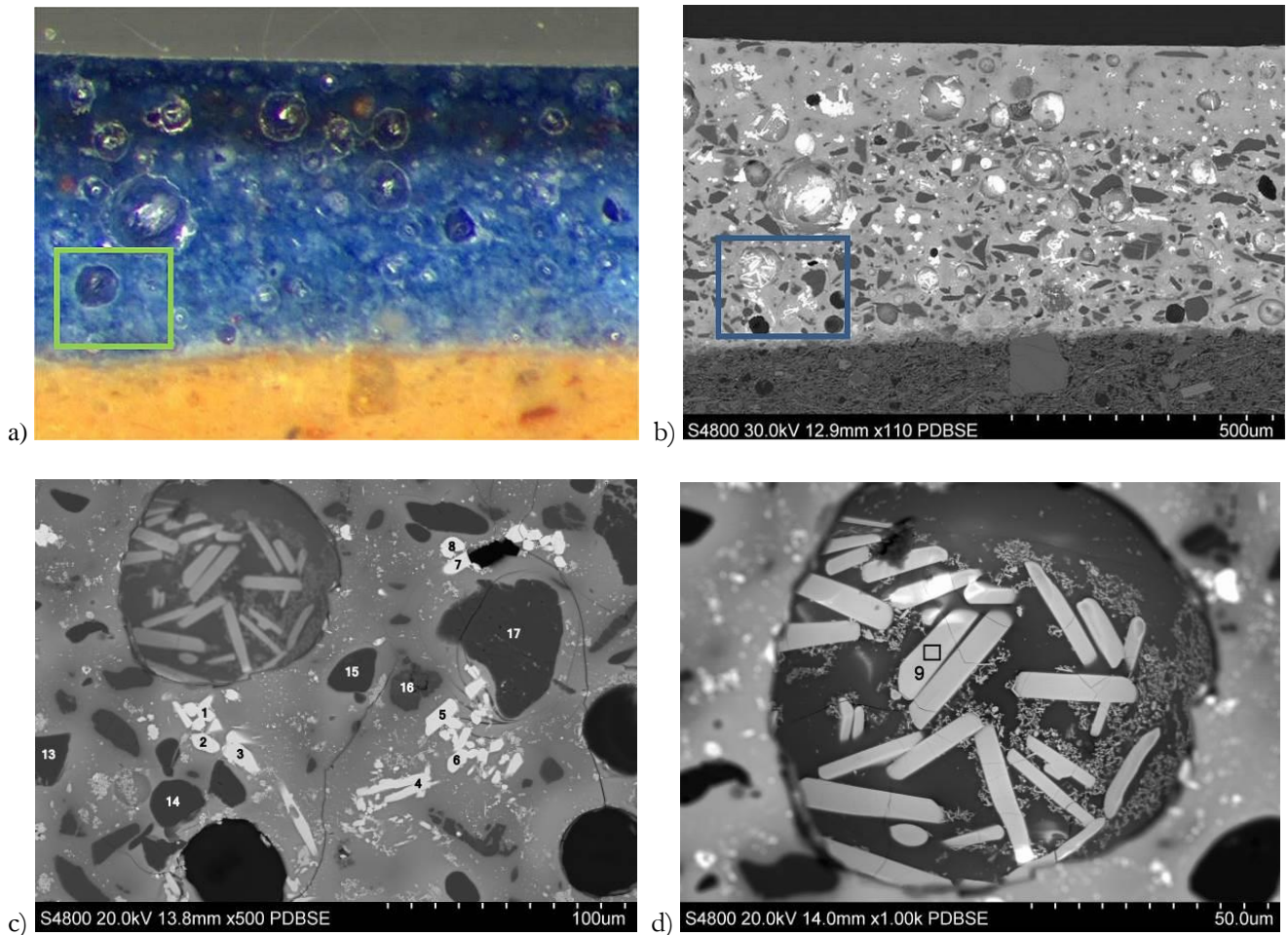
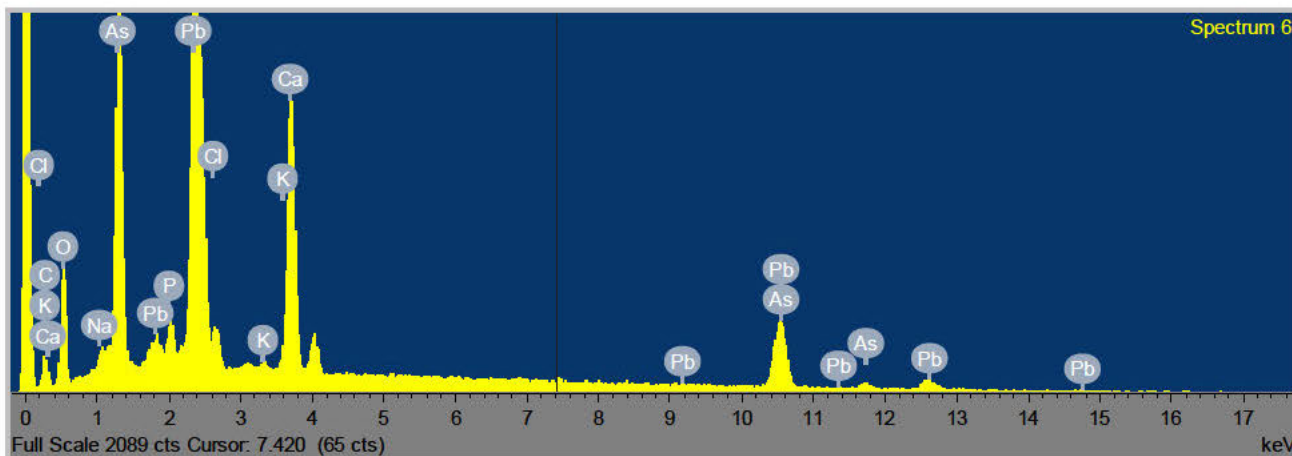


Figure 19. Sample TW01: a) & b) areas outlined in which large calcium-lead arsenate crystals ($30 \mu\text{m}$ long) and mineral grains are found in the lower glaze c), detail d) note also the tiny tin oxide particles adjacent to the large arsenate crystals.

Table 6a. Large calcium lead arsenate crystals (white) in Figure 19.

wt% oxides	CaO	As ₂ O ₃	PbO	Atomic % elements	Ca	As	Pb	O
Mean of spectra 1-9	23.0	34.7	42.3	Mean	19.7	16.9	9.2	54.2



Spectrum 6. Ca, As, Pb. Note the distinguishing large arsenic peak 'La' line at 1.282 keV and smaller 'Kβ1' at 11.724keV.

Table 6b. Larger (dark) mineral grains and associated spectra in the glaze of Figure 19.

Surface minerals wt% oxide	Si	K	Al
Spectra 13-15 & 17 mean. Quartz	99.9	0.0	0.1
Spectrum 16. Feldspar	64.0	13.2	19.1

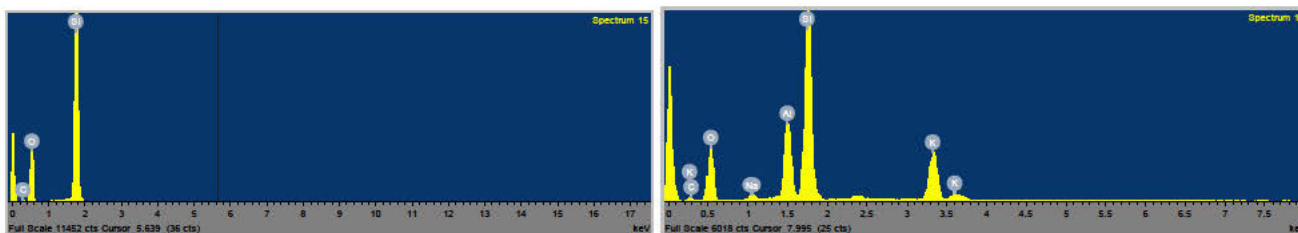


Figure 20. TW01, quartz and feldspar spectra from Table 6b, spectrum 15. Left: Si, O (quartz). Note how 'clean' the spectrum is from this 20 μm size quartz grain, with no beam penetration scatter effects from the glass matrix as the whole beam is fully 'captured' within the confines of the grain. Right: spectrum 16, feldspar grain containing only K, Al, Si, O.



Figure 21. TW01: map sum spectrum - detail of bismuth X-ray energy line peaks, particularly the unique Bi La1 and Lb1 lines.

Other individual mineral grains analysed within the glaze in Figure 19 are of quartz and feldspar that give very specific spectral signatures (Table 6b, and Figure 20 spectra 15 and 16 respectively). These mineral grains are clearly seen in the Si, Al, K elemental maps of Figures 8 and 9, particularly within the opacified lower glaze. The quartz and feldspar result from the addition of sand to the fritted glazing mixture.

Bismuth

Bismuth (Bi) appears in the glaze analyses and the sum map spectra: EDX principal X-ray emission line peaks of bismuth, Bi $L\alpha_1$ @ 10.838 keV and Bi $L\beta_1$ @ 13.023 keV (Kortright and Thompson 2001) (Figure 21). This line is unique to bismuth and does not overlap with lead or arsenic, whereas some other 'L' line peaks do. These $L\alpha_1$ and $L\beta_1$ line peaks confirm the presence of bismuth in significant amounts. Bismuth is most likely a contaminant along with arsenic in the cobalt ore (Zucchiatti *et al.* 2006). It was not possible at this moment to provide an element map for bismuth, but further investigation might provide one.

CONCLUSIONS

The combination of detailed digital SEM-EDX high-resolution elemental X-ray maps of polished cross sections, combined with high-resolution FE-SEM imaging and analyses, along with colour optical microscopy images of the maiolica bodies and complex glazes, has extended our ability to identify the phases and minerals present in the paste and glaze and to understand the reactions that have occurred during the two-phase glaze production. Presentation of these data from complex ceramics as colour concentration maps with associated mineral spectral analysis and BSE grey level images provides important visualisation of the minerals in the fabric - spatially, qualitatively and quantitatively.

In summary, the strengths of this technique are visible in the investigation of both maiolica body and glaze, which allowed us to examine in detail:

- 1) the mineral phases of the maiolica body present in the clay, which are identifiable by mapping and microanalysis together with their morphology, size and distribution seen in BSE images; this information has the potential for a more general application to identify and group ceramic objects made from clay from the same source (i.e. provenance studies);
- 2) the clay particles within the paste, which show typical vitrification within glassy filaments that form through fusion to the mineral phases (here the potential for further studies using high-resolution microscopy and microanalysis of the glassy filaments and observation of their relationship with clay particles and minerals is proven); and
- 3) the distribution of the calcium aluminium silicate phases formed as a result of the reaction between the clay minerals and the calcite present in the original calcareous clay is established for the maiolica.

Similarly, the analyses of the maiolica glazes provide detailed information on:

- 1) the mineral phases present in the sand added to the fritted glazing mixture (quartz and feldspars) in the primary glazed layer, and their absence in the overlying, *coperta* glaze layer. The compositional maps help considerably in the identification of the complexity and distribution of the various high atomic number phases visible in the high-resolution SEM BSE images of the glaze (i.e. phases appearing relatively bright or white in the images). Thus, the tin oxide particles that provide the opacification can be seen as sub-micron particles grouped in larger assemblages and distinguished from both the remnant particles of cobalt pigment and the calcium lead arsenate particles and confirmed from elemental map concentrations and subsequent analyses of the phases extracted from the map data;
- 2) the cobalt blue glaze colouration, and the association between cobalt, arsenic, nickel and iron is established, much of which has been retained in the remnant pigment mineral particles in a band at the interface between the two glaze layers where the particles of finely ground crushed ore were added to the surface of the first glaze and then overfired with the second transparent glaze. The cobalt has diffused from the pigment ore particles throughout both of the glaze layers along with nickel in equivalent proportions, whereas the iron diffusion remains largely concentrated in the middle-banded region. This information, as well as the presence of arsenic, is crucial in identifying the Erzgebirge region in Saxony as the probable source of the cobalt pigment (Zucchiatti *et al.* 2006, 148; Tite 2009, 2077); and
- 3) the arsenic distribution (a contaminant of the cobalt mineral) which has similarly diffused throughout the outer and inner glaze layers during glaze firing, but is also present in

specific acicular calcium/lead arsenate crystalline form in both of the glaze layers as a by-product of glazing chemistry.

The ability to revisit primary data using off-line processing software from the original digital EDX analytical system is essential to enhance our interpretations and answer new questions. More recent developments in SEM-EDX mineral identification software are available as the technology develops from more general geological applications (<https://nano.oxinst.com/application-detail/geology-petrology-and-mining/>).

Element legend

O oxygen
Na sodium
Mg magnesium
Al aluminium
Si silicon
K potassium
Ca calcium
Ti titanium
Mn manganese
Fe iron
Co cobalt
Ni nickel
Sn tin
Pb lead
As arsenic
Bi bismuth

References

- Freestone, I. C. 1982. Applications and potential of Electron Probe Micro-Analysis in technological and provenance investigations of ancient ceramics. *Archaeometry* 24, 2, 99-116.
- Goldstein, J., Newbury, D. E., Joy, D. C., Lyman, C. E., Echlin, P., Lifshin, E., Sawyer, L. and Michael, J. R. 2003. *Scanning Electron Microscopy and X-Ray Microanalysis. Third edition.* Springer.
- Goldstein, J. I., Newbury, D. E., Michael, J. R., Ritchie, N. W. M., Scott, J. H. J and Joy, D. C. 2018. *Scanning Electron Microscopy and X-Ray Microanalysis. Fourth edition.* Springer.
- Kortright, J. B. and Thompson, A. C. 2001. X-Ray Emission Energies, in Thompson, A. C. and Vaughan, D. (eds.), *X-Ray Data Booklet*, section 1.2 X-Ray Properties of the Elements, Center for X-ray Optics and Advanced Light Source, Lawrence Berkeley National Laboratory.
- <https://physics.uwo.ca/~lgonchar/courses/p9826/xdb.pdf>
- Lyman, C. E., Newbury, D. E., Goldstein, J., Williams, D. B., Romig Jr., A. D., Armstrong, J., Echlin, P., Fiori, C., Joy, D. C., Lifshin, E., and Peters, K. R. 1990. *Scanning Electron Microscopy, X-Ray Microanalysis, and Analytical Electron Microscopy: A Laboratory Workbook.* Springer.
- Meeks, N. D. 1988. Backscattered electron imaging of archaeological material. In Olsen S. L. (ed.) *Scanning Electron Microscopy in Archaeology.* BAR International Series 452, pp. 23-44.
- Molera, J., Pradell, T., Salvadó, N. and Vendrell-Saz, M. 1999. Evidence of Tin Oxide Recrystallization in Opacified Lead Glazes. *Journal of American Ceramic Society* 82, 2871-2875.
- Oxford Instruments Nanoanalysis *Application Notes:* <https://nano.oxinst.com/campaigns/downloads/large-area-eds-mapping-phase-distribution-in-archaeological-samples>
<https://nano.oxinst.com/application-detail/geology-petrology-and-mining/>
<https://nano.oxinst.com/products/aztec/aztecmineral>
- Piccolpasso, C. ca. 1557. *Li tre libri dell'arte del vasaio.* Italy, Castel Durante (now Urbania), Treatise on maiolica, Victoria and Albert Museum no. MSL/1861/7446, folio 14 recto.
- Russ, J. C. 2013. *Fundamentals of Energy Dispersive X-Ray Analysis: Butterworths Monographs in Materials.* Butterworth-Heinemann.
- Statham, P. J. 1998. Recent Developments in Instrumentation for X-Ray Microanalysis. In Love, G., Nicholson, W.A.P. and Armigliato, A. (eds.) *Modern Developments and Applications in Microbeam Analysis. Mikrochimica Acta Supplement, vol 15.* Springer, Vienna.
- Tite, M. S., Freestone, I., Mason, R., Molera, J., Vendrell-Saz, M. and Wood, N. 1998. Lead glazes in antiquity - methods of production and reasons for use. *Archaeometry* 40, 241-260.
- Tite, M. S. 2009. The production technology of Italian maiolica: a reassessment. *Journal of Archaeological Science* 36(10), 2065-2080.
- Tite, M. S. 2012. Italian Maiolica. *The Old Potter's Almanack, Volume 17 (2)*, December 2012.

Zucchiattiz, A., Bouquillon, A., Katona, I. and D'Alessandro, A. 2006. The 'della Robbia blue': A case study for the use of cobalt pigments in ceramics during the Italian Renaissance. *Archaeometry* 48(1), 131 – 152.

Further reading

Peruzzo, L., Fenzi, F. and Vigato, P. A. 2011. Electron backscatter diffraction (EBSD): a new technique for the identification of pigments and raw materials in historic glasses and ceramics. *Archaeometry* 53(1), 178-193, Wiley Online Library.

Procop, M., Hodoroaba, V. D., Bjeoumikhov, A., Wedell, R. and Warrikhoff, A. 2009. Improvements of the low-energy performance of a micro-focus x-ray source for XRF analysis with the SEM. *X-ray Spectrometry* 38(4), 308-311.

Williams, D. B., Goldstein, J. I. and Newbury, D. E. (eds.). 1995. *X-Ray Spectrometry in Electron Beam Instruments*, Plenum Press, NY.

Stokes, D. J. 2008 *Principles and Practice of Variable Pressure/Environmental Scanning Electron Microscopy (VP-ESEM)*. John Wiley & Sons, Ltd.

X-ray Emission Energies:

https://www.horiba.com/fileadmin/uploads/Scientific/Documents/XRay/emission_lines.pdf
